IEEE Photonics Journal
An IEEE Photonics Society Publication

Open Access

Energy-Stable Time-Domain Finite Element Methods for the 3D Nonlinear Maxwell's Equations

Volume 12, Number 2, April 2020

Asad Anees, ***Member, IEEE***
Lutz Angermann

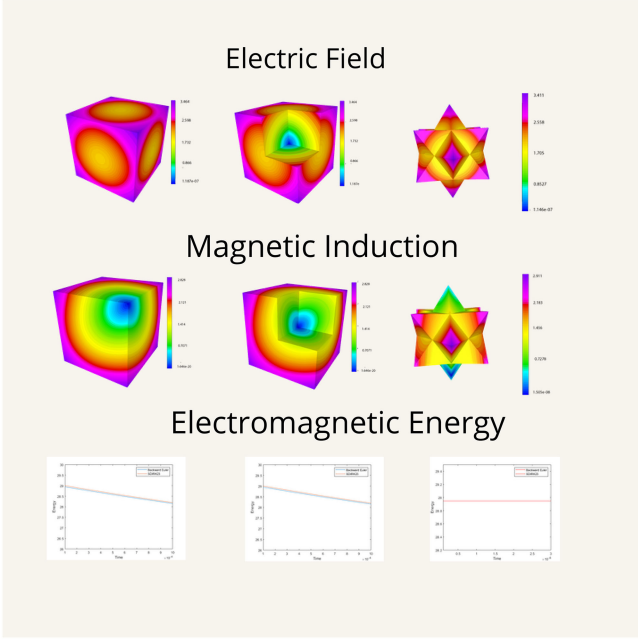

DOI: 10.1109/JPHOT.2020.2977233

IEEE photonics SOCIETY
IEEE

Energy-Stable Time-Domain Finite Element Methods for the 3D Nonlinear Maxwell's Equations

Asad Anees [1,2] ***Member, IEEE***, **and Lutz Angermann** [1]

[1] Institute of Mathematics, Clausthal University of Technology, D-38678 Clausthal-Zellerfeld, Germany
[2] Department of Mathematics and Statistics, University of Agriculture Faisalabad, Punjab 38000, Pakistan

DOI:10.1109/JPHOT.2020.2977233

Manuscript received February 4, 2020; accepted February 25, 2020. Date of publication February 28, 2020; date of current version March 26, 2020. This work was supported in part by the German Academic Exchange Service (DAAD) under Grant 57129429, and in part by the Open Access Publishing Fund of Clausthal University of Technology. Corresponding author: Asad Anees (e-mail: asad.anees@tu-clausthal.de; asadanees@uaf.edu.pk).

Abstract: In this paper, time-domain finite element methods for the full system of Maxwell's equations with cubic nonlinearities in 3D are presented, including a selection of computational experiments. The new capabilities of these methods are to efficiently model linear and nonlinear effects of the electrical polarization. The novel strategy has been developed to bring under control the discrete nonlinearity model in space and time. It results in energy stable discretizations both at the semi-discrete and the fully discrete levels, with spatial discretization using edge and face elements (Nédeléc-Raviart-Thomas formulation). In particular, the proposed time discretization schemes are unconditionally stable with respect to a specially defined nonlinear electromagnetic energy, which is an upper bound of the electromagnetic energy commonly used. The approaches presented prove to be robust and allow the modeling of 3D optical problems that can be directly derived from the full system of Maxwell's nonlinear equations, and allow the treatment of complex nonlinearities and geometries of various physical systems coupled with electromagnetic fields.

Index Terms: Finite element analysis, nonlinear maxwell's equations, backward euler method, SDIRK method, energy stability, computational modeling, visualization.

1. Introduction

Nonlinear Optics deals with phenomena that occur when the optical properties of a material change under the action of light. It is a key technology for optical communication, data processing and storage. Nonlinear optical phenomena are nonlinear in the sense that the response of the medium to the light is nonlinearly dependent on its intensity. Frequently, the behavior of light waves in a material is modeled by means of a third-order polarization response, that is the polarization $\mathbf{P}(\mathbf{E})$ is a cubic polynomial of the electric field intensity $\mathbf{E}$. This modeling approach is widely accepted for not too small, but still moderate intensities. At very high intensities, which shall not be considered here, it is no longer adequate. The books [1]–[4] describe the fundamental concepts of nonlinear Optics.

Since the investigation of light propagation in nonlinear materials involves the solution of nonlinear partial differential equations, various numerical methods for approximating the solutions

dominate the practice, for instance finite difference time-domain (FDTD) methods, slowly varying envelope approximations (SVEA), beam propagation methods (BPM), time-domain finite element methods (TDFEM) – among them time-domain discontinuous Galerkin (TDdG) methods –, pseudo-spectral methods, finite volume methods (FVM) (sometimes also called finite integration techniques (FIT)), and many more.

The more conventional FDTD methods are regarded as robust simulation schemes for linear and nonlinear models in Optics and Photonics [5]–[13], but also generally in the field of Computational Electromagnetism, although there are considerable limitations in terms of applicability to complicated geometries, less smooth data (e.g. caused by material interfaces), etc. Typically the spatial domain is discretized by regular, structured (quadrilateral or hexahedral), staggered grids. The difference scheme presented in [5] served as the basis for one of the most commonly-used methods to solve the linear Maxwell's equations. This scheme is of second order in time and exhibits a significant numerical dispersion over long time interval of wave propagation simulation [12]. FDTD simulations for the full system of nonlinear Maxwell's equations have been presented in [7], [8]. Among other things, interacting waves of different frequencies could be treated directly [8]. The auxiliary differential equation (ADE) method along with finite difference time-domain (FDTD) schemes has been originally employed for linear dispersive materials [6] and for the coupling between the polarization vector and the electric field intensity [7], [14]. This scheme was applied to second- and third-order nonlinear phenomena including spatial soliton propagation [14], [15], linear and nonlinear interface scattering [16], and pulse propagation through nonlinear wave guides [17]. A lot of interesting modeling and simulation results for linear and nonlinear Lorentz dispersion with nonlinear Kerr response in case of 1D, 2D and 3D can be found in [15], [18]–[23]. Among non-standard difference methods, pseudospectral spatial domain schemes have been employed for optical carrier shock [24] and linear Lorentz dispersion with nonlinear response [25] simulation.

Slowly varying envelope approximations (SVEA) are mostly used to simulate effects in nonlinear Photonics. Using this scheme, the system of Maxwell nonlinear equations transforms into the nonlinear Schrdinger equation. Various nonlinear effects such as self phase modulation and the Kerr effect can be successfully numerically treated [1], [26]. The beam propagation method (BPM) with second-order indices of refraction is employed for modeling of nonlinear optical devices exhibiting on-axis behaviour [27].

Finite volume methods have been applied to nonlinear Kerr media in 1D and 2D cases [28], [29]. For the Maxwell's equations with Kerr-type nonlinearity, a hyperbolic system is derived and approximated by the Godunov method. Moreover a higher-order Roe solver is also employed for simulations.

In the past few years, discontinuous Galerkin methods have attracted considerable attention and are now being applied to a wide range of problems from hydrodynamics to acoustics and electrodynamics. To the authors' knowledge, the first mathematical proof for the convergence of the discontinuous Galerkin method when applied to Maxwell's equations was given in the paper [30]. The methods allow a comparatively easy handling of elements of various types and shapes, irregular non-conforming meshes and even locally varying polynomial degree. For the linear situation the papers [31]–[34] can be mentioned as examples, for dispersive media we refer to [35], [36]. For the system of Maxwell's equations with material nonlinearities, there are still very few rigorous analysis, error estimates, and simulation results using time domain finite element methods ((TDFEM/TDdG) available [26], [37]–[46]. In the paper [43] a higher-order discontinuous Galerkin method is used to discretize the problem in space. Two time discretization schemes are investigated – a second-order leapfrog and the implicit trapezoidal scheme. In the fully discretized problems, the nonlinearity is treated by employing the auxiliary differential equation (ADE) approach. In [43] it has been proved that the first scheme is conditionally stable, while the fully implicit method is unconditionally stable. The results for the proposed schemes were given only for the 1D case, and error estimates were obtained only for the semi-discrete problem under some additional assumptions on the strength of the nonlinearity.

In this paper, we present a novel technique to solve the 3D nonlinear problem in Optics and Photonics. We extend the semi-discrete mixed finite element method [47], [48] and the fully discrete

finite element method [49], [50] to the fully time-dependent Maxwell's equations with nonlinearities. The electric and magnetic fields in the Maxwell's equations with a cubic nonlinearity are discretized in space by means of pairs of Nédeléc curl-conforming and Raviart-Thomas div-conforming finite elements. The spatial discretization has all the well-known properties of these spaces [51]–[53], especially a high accuracy and the ability to handle complex geometries. In addition, we are able to demonstrate that the semi-discrete and fully discrete solutions have similar energy-conserving propertie as the exact solution. The backward Euler-type and SDIRK solvers are used to discretize the problem in the time domain. We also present fully discrete schemes for the nonlinear problem in 3D that possess the property of energy stability and are unconditionally stable. Achieving these results required a careful modeling of the nonlinearities in the fully discrete scheme by a suitable application of the auxiliary differential equation (ADE) approach. The energy stability properties are important in the sense that they reflect the physical behaviour of the exact solution and make the schemes robust.

Let Ω be a smooth, simply connected domain in $\mathbb{R}^3$ with boundary $\partial\Omega$ and unit outward normal $\mathbf{n}$. Let $\mathbf{D} = \mathbf{D}(\mathbf{x}, t)$, $\mathbf{B} = \mathbf{B}(\mathbf{x}, t)$, $\mathbf{E} = \mathbf{E}(\mathbf{x}, t)$ and $\mathbf{H} = \mathbf{H}(\mathbf{x}, t)$ represent the displacement field, magnetic induction, electric and magnetic field intensities respectively, where $\mathbf{x} \in \Omega$ and the time variable t ranges in some interval $(0, T)$, $T > 0$. Given an electric current density $\mathbf{J} = \mathbf{J}(\mathbf{x}, t)$, we write the time-dependent Maxwell's equations as

$$\partial_t \mathbf{D} - \nabla \times \mathbf{H} = \mathbf{J} \text{ in } \Omega \times (0, T), \tag{1}$$

$$\partial_t \mathbf{B} + \nabla \times \mathbf{E} = 0 \text{ in } \Omega \times (0, T), \tag{2}$$

where the following constitutive relations hold:

$$\mathbf{B} := \mu_0 \mathbf{H} \quad \text{and} \quad \mathbf{D} := \varepsilon_0 \mathbf{E} + \mathbf{P}(\mathbf{E}). \tag{3}$$

$\varepsilon_0 > 0$ and $\mu_0 > 0$ are the vacuum permittivity and permeability respectively. Often the nonlinear constitutive relation for the polarization $\mathbf{P} = \mathbf{P}(\mathbf{E})$ is approximated by a truncated Taylor series [1]. In case of an isotropic material, it takes the form,

$$\mathbf{P}(\mathbf{E}) := \varepsilon_0 \left(\chi^{(1)} \mathbf{E} + \chi^{(3)} \mathbf{E}^3 \right), \tag{4}$$

where, in general, $\chi^{(i)} : \Omega \to (\mathbb{R}^3)^{i+1}$ are the media susceptibility tensors $i = 1, 3$. Here we further restrict the model to more symmetric materials so that the second term in (4) takes the form $\chi^{(3)} |\mathbf{E}|^2 \mathbf{E}$ with a nonnegative scalar coefficient $\chi^{(3)} : \Omega \to \mathbb{R}$. We also assume that $\chi^{(1)}$ is a positive scalar coefficient $\chi^{(1)} : \Omega \to \mathbb{R}$. For $\chi^{(3)} = 0$, we obtain the linear Maxwell's equations. Thus the nonlinear Maxwell's equations (1)–(4) can be rewritten as:

$$\partial_t \mathbf{D} - \nabla \times \mathbf{H} = \mathbf{J} \text{ in } \Omega \times (0, T), \tag{5}$$

$$\mu_0 \partial_t \mathbf{H} + \nabla \times \mathbf{E} = 0 \text{ in } \Omega \times (0, T), \tag{6}$$

where

$$\partial_t \mathbf{D} = \varepsilon_0 \left(1 + \chi^{(1)} + \chi^{(3)} |\mathbf{E}|^2 + 2\chi^{(3)} \mathbf{E}\mathbf{E}^T \right) \partial_t \mathbf{E}. \tag{7}$$

On $\partial\Omega$ a perfect conducting boundary condition is assumed: $\mathbf{n} \times \mathbf{E}|_{\partial\Omega} = 0$. In addition, initial conditions have to be specified so that $\mathbf{E}(\mathbf{x}, 0) = \mathbf{E}_0(\mathbf{x})$ and $\mathbf{H}(\mathbf{x}, 0) = \mathbf{H}_0(\mathbf{x})$ for all $\mathbf{x} \in \Omega$, where $\mathbf{E}_0$ and $\mathbf{H}_0$ are given functions on Ω, and $\mathbf{H}_0$ satisfies $\nabla \cdot \mu_0 \mathbf{H}_0 = 0$ in Ω, $\mathbf{H}_0 \cdot \mathbf{n} = 0$ on $\partial\Omega$. Concerning the function spaces and related notation, we refer to [53]–[56] for details; a short summary can be found in [50, Section II].

The paper is structured as follows. Sections 2 and 3 describe the weak formulation and the spatial discretization of the nonlinear problem. The time discretization and energy at the fully discrete level are discussed in Section 4. Finally, Section 5 presents a collection of numerical experiments.

2. A Weak Formulation

The test by functions $\boldsymbol{\Psi} \in \mathbf{H}_0(\mathrm{curl}\,;\Omega)$, $\boldsymbol{\Phi} \in \mathbf{V} = \mathbf{H}(\mathrm{div};\Omega)$ and integration by parts in the equation (5) leads to a weak formulation w.r.t. $(\mathbf{E},\mathbf{H}) \in C^1(0,T,\mathbf{H}_0(\mathrm{curl}\,;\Omega)) \times (C(0,T,\mathbf{H}_0(\mathrm{curl}\,;\Omega)) \cap C^1(0,T,\mathbf{L}^2_{\varepsilon_0(1+\chi^{(1)})}(\Omega))) \times (C(0,T,\mathbf{H}(\mathrm{div};\Omega)) \cap C^1(0,T,\mathbf{L}^2(\Omega)))$ of (5)–(7) such that

$$(\partial_t \mathbf{D},\boldsymbol{\Psi}) - (\mathbf{H},\nabla\times\boldsymbol{\Psi}) = (\mathbf{J},\boldsymbol{\Psi}) \qquad \forall\,\boldsymbol{\Psi}\in\mathbf{H}_0(\mathrm{curl}\,;\Omega), \tag{8}$$

$$\begin{aligned}(\partial_t \mathbf{D},\boldsymbol{\Psi}) &= (\varepsilon_0(1+\chi^{(1)})\partial_t\mathbf{E},\boldsymbol{\Psi}) + \left(\varepsilon_0\chi^{(3)}\left(|\mathbf{E}|^2\,\partial_t\mathbf{E}\right),\boldsymbol{\Psi}\right)\\ &\quad + 2\left(\varepsilon_0\chi^{(3)}\left([\mathbf{E}\mathbf{E}^T]\,\partial_t\mathbf{E}\right),\boldsymbol{\Psi}\right) \qquad \forall\,\boldsymbol{\Psi}\in\mathbf{H}_0(\mathrm{curl}\,;\Omega),\end{aligned} \tag{9}$$

$$(\mu_0\partial_t\mathbf{H},\boldsymbol{\Phi}) + (\nabla\times\mathbf{E},\boldsymbol{\Phi}) = 0 \qquad \forall\,\boldsymbol{\Phi}\in\mathbf{H}(\mathrm{div};\Omega). \tag{10}$$

In addition, the following initial conditions have to be satisfied:

$$\mathbf{E}(\mathbf{x},0) = \mathbf{E}_0(\mathbf{x}) \quad \text{and} \quad \mathbf{H}(\mathbf{x},0) = \mathbf{H}_0(\mathbf{x}), \quad \mathbf{x}\in\Omega. \tag{11}$$

The nonlinear electromagnetic energy of the system (8)–(10) at any time t is defined by

$$\textbf{Energy} := \|\mathbf{E}(t)\|^2_{\varepsilon_0(1+\chi^{(1)})} + \frac{3}{2}\|\mathbf{E}^2(t)\|^2_{\varepsilon_0\chi^{(3)}} + \|\mathbf{H}(t)\|^2_{\mu_0}.$$

It can be shown that the nonlinear electromagnetic energy at any time t is bounded by the initial energy plus the energy introduced through $\mathbf{J}$. In the absence of the source term $\mathbf{J}$, an exact energy conservation law even holds.

3. Spatial Discretization

Let $\mathbf{U}_{0h} \subset \mathbf{H}_0(\mathrm{curl}\,;\Omega)$, and $\mathbf{V}_h \subset \mathbf{V}$ be finite-dimensional subspaces (as usual, $h>0$ denotes a typical mesh size parameter). For details about the finite element subspaces, curl-conforming and div-conforming elements see, e.g., the spatial discretization in [50, Section IV, equations (19)–(23)].

For the equations (8)–(10), the semi-discrete problem involves the determination of elements $(\mathbf{D}_h,\mathbf{E}_h,\mathbf{H}_h) \in C^1(0,T,\mathbf{U}_{0h}) \times C^1(0,T,\mathbf{U}_{0h}) \times C^1(0,T,\mathbf{V}_h)$ satisfying

$$(\partial_t \mathbf{D}_h,\boldsymbol{\Psi}_h) - (\mathbf{H}_h,\nabla\times\boldsymbol{\Psi}_h) = (\mathbf{J}_h,\boldsymbol{\Psi}_h) \qquad \forall\boldsymbol{\Psi}_h\in\mathbf{U}_{0h}, \tag{12}$$

$$\begin{aligned}(\partial_t \mathbf{D}_h,\boldsymbol{\Psi}) &= (\varepsilon_0(1+\chi^{(1)})\partial_t\mathbf{E}_h,\boldsymbol{\Psi}_h) + \left(\varepsilon_0\chi^{(3)}\left(|\mathbf{E}_h|^2\,\partial_t\mathbf{E}_h\right),\boldsymbol{\Psi}_h\right)\\ &\quad + 2\left(\varepsilon_0\chi^{(3)}\left([\mathbf{E}_h\mathbf{E}_h^T]\,\partial_t\mathbf{E}_h\right),\boldsymbol{\Psi}_h\right) \qquad \forall\,\boldsymbol{\Psi}_h\in\mathbf{U}_{0h},\end{aligned} \tag{13}$$

$$(\mu_0\partial_t\mathbf{H}_h,\boldsymbol{\Phi}_h) + (\nabla\times\mathbf{E}_h,\boldsymbol{\Phi}_h) = 0 \qquad \forall\boldsymbol{\Phi}_h\in\mathbf{V}_h. \tag{14}$$

The initial conditions read formally as

$$\mathbf{E}_h(\mathbf{x},0) = \mathbf{E}_{0h}(\mathbf{x}) \quad \text{and} \quad \mathbf{H}_h(\mathbf{x},0) = \mathbf{H}_{0h}(\mathbf{x}), \quad \mathbf{x}\in\Omega,$$

where $\mathbf{E}_{0h}\in\mathbf{U}_{0h}$, $\mathbf{H}_{0h}\in\mathbf{V}_h$ are approximations to $\mathbf{E}_0$, $\mathbf{H}_0$.

The nonlinear electromagnetic energy at the semi-discrete level of the system (12)–(14) at time t is defined by

$$\textbf{Energy}_h := \|\mathbf{E}_h\|^2_{\varepsilon_0(1+\chi^{(1)})} + \frac{3}{2}\|\mathbf{E}_h^2\|^2_{\varepsilon_0\chi^{(3)}} + \|\mathbf{H}_h\|^2_{\mu_0}.$$

Similar to the situation in Section 2 it is possible to show that the nonlinear electromagnetic energy at the semi-discrete level of the system (12)–(14) at time t is bounded, and an exact energy conservation law is satisfied if $\mathbf{J}=0$.

Hence the semi-discrete solution has analogous energy-conserving properties as the exact solution.

4. Time Discretization

In this section, we present novel fully discrete schemes for the nonlinear Maxwell's equations. Our particular interest is to demonstrate that the time discretizations by means of the classical backward Euler-type and singly diagonally implicit Runge-Kutta methods satisfy a discrete energy estimate, are unconditionally stable and convergent even in the presence of cubic nonlinearities. Analogous investigations for the linear case (that is $\chi^{(3)} = 0$) have already been presented in [50]. The time discretization considered here can be used not only in conjunction with the Nédeléc and Raviart-Thomas spatial discretizations, but also with other types of spatial discretizations. The Newton's method is often employed to obtain the unknown values $\mathbf{E}_h^n$ and $\mathbf{H}_h^n$ from the nonlinear equations (15)–(17).

We divide the time interval $(0, T)$ into $N \in \mathbb{N}$ equally spaced subintervals by using the nodal points

$$0 =: t^0 < t^1 < t^2 < \ldots < t^N := T,$$

with $t^n = n\Delta t$, $n = 0, 1, 2, \ldots, N$.

4.1 The Fully Discrete Scheme for the Nédeléc and Raviart-Thomas Formulation

Here we prescribe initial values $(\mathbf{E}_h^0, \mathbf{H}_h^0) \in \mathbf{U}_{0h} \times \mathbf{V}_h$ of the approximate electric and magnetic field intensities and determine the fully discrete electric and magnetic field intensities $(\mathbf{E}_h^n, \mathbf{H}_h^n) \in \mathbf{U}_{0h} \times \mathbf{V}_h$, $n = 1, 2, \ldots, N$, such that the following system is satisfied:

$$\left(\frac{\mathbf{D}_h^n - \mathbf{D}_h^{n-1}}{\Delta t}, \boldsymbol{\Psi}_h\right) - (\mathbf{H}_h^n, \nabla \times \boldsymbol{\Psi}_h) = (\mathbf{J}_h^n, \boldsymbol{\Psi}_h) \qquad \forall\, \boldsymbol{\Psi}_h \in \mathbf{U}_{0h}, \quad (15)$$

$$\begin{aligned}(\mathbf{D}_h^n - \mathbf{D}_h^{n-1}, \boldsymbol{\Psi}_h) &= (\varepsilon_0(1+\chi^{(1)})\left(\mathbf{E}_h^n - \mathbf{E}_h^{n-1}\right), \boldsymbol{\Psi}_h) \\ &\quad + \frac{1}{2}\varepsilon_0\chi^{(3)}(((\mathbf{E}_h^n)^2 + (\mathbf{E}_h^{n-1})^2)\left(\mathbf{E}_h^n - \mathbf{E}_h^{n-1}\right), \boldsymbol{\Psi}_h) \\ &\quad + \left(\varepsilon_0\chi^{(3)}\left[\mathbf{E}_h^n\left[\mathbf{E}_h^n\right]^T + \mathbf{E}_h^{n-1}\left[\mathbf{E}_h^{n-1}\right]^T\right]\left(\mathbf{E}_h^n - \mathbf{E}_h^{n-1}\right), \boldsymbol{\Psi}_h\right) \qquad \forall\, \boldsymbol{\Psi}_h \in \mathbf{U}_{0h}, \quad (16)\end{aligned}$$

$$\left(\mu_0\frac{\mathbf{H}_h^n - \mathbf{H}_h^{n-1}}{\Delta t}, \boldsymbol{\Phi}_h\right) + (\nabla \times \mathbf{E}_h^n, \boldsymbol{\Phi}_h) = 0 \qquad \forall\, \boldsymbol{\Phi}_h \in \mathbf{V}_h. \quad (17)$$

The differences $\mathbf{D}_h^n - \mathbf{D}_h^{n-1}$ play the role of auxiliary variables. In addition, the fully discrete formulation is not subject to any size limit w.r.t. $\Delta t/h$.

Remark 1: (i) If μ is variable, in particular jumps, it makes more sense to use the $(\mathbf{E}, \mathbf{B})$ formulation instead of $(\mathbf{E}, \mathbf{H})$.

(ii) A full discretization can be defined similar by employing the SDIRK23 method (singly diagonally implicit Runge-Kutta method) for the nonlinear problem (12)–(14), the difference of auxiliary variable $\mathbf{D}_h^n - \mathbf{D}_h^{n-1}$ is indeed same.

The nonlinear electromagnetic energy for the fully discrete approximation (i.e. both in space and time) of the system (15)–(17) at t^n, $n = 0, 1, 2, \ldots, N$, is defined by

$$\mathbf{Energy}_h^n := \|\mathbf{E}_h^n\|^2_{\varepsilon_0(1+\chi^{(1)})} + \frac{3}{2}\|(\mathbf{E}_h^n)^2\|^2_{\varepsilon_0\chi^{(3)}} + \|\mathbf{H}_h^n\|^2_{\mu_0}. \quad (18)$$

In analogy to the boundedness results for the continuous and semi-discrete nonlinear electromagnetic energy, it can be seen that the fully discrete nonlinear electromagnetic energy of the system (15)–(17) at the final time step N is bounded and conserved, too. Furthermore, the fully discrete solution has similar energy-conserving properties as the exact solution. Similar energy conservation properties can be obtained numerically for high-order time domain methods e.g. leapfrog, SDIRK23 and symplectic schemes coupled with semi-discrete scheme from Section 3.

5. Numerical Results, Validations and Discussion

The nonlinear electromagnetic energy (18) for the fully discretized problem (15)–(17) will be verified by a number of computational experiments for different material values. Furthermore, our proposed semi-discretization is tested by the two-stage SDIRK23 method [57], [58] (singly diagonally implicit Runge-Kutta method). SDIRK23 is an L-stable and second order method.

The full discretization of the system of nonlinear partial differential equations (5)–(7) leads to the nonlinear system of difference equations (15)–(17), which is solved by means of Newton's method. It is very important to reduce the computational costs associated with nonlinear iterations required to achieve the convergence. The computational costs connected with nonlinear iterations are minimized by our proposed time discretization. Thanks to the special structure of the time-discretized nonlinearity, at each time step the Newton iterations reduce to a single Euler-like backward step, making the whole procedure competitive. Let $\mathbf{e}^n$ and $\mathbf{h}^n$ be the algebraic representation vectors of $\mathbf{E}_h^n$ and $\mathbf{H}_h^n$, respectively. The vector $\mathbf{j}^n$ denotes the discrete current source density. First we compute the representation vector $\mathbf{d}^n - \mathbf{d}^{n-1}$ of the auxiliary variable $\mathbf{D}_h^n - \mathbf{D}_h^{n-1}$ that is defined in the fully discrete formulation (16). It can be simplified as:

$$\begin{aligned}\mathbf{d}^n - \mathbf{d}^{n-1} &= \mathbf{M}_{\varepsilon_0(1+\chi^{(1)})}(\mathbf{e}^n - \mathbf{e}^{n-1}) + \mathbf{M}_{\varepsilon_0\chi^{(3)}\|\mathbf{e}\|^2}(\mathbf{e}^n - \mathbf{e}^{n-1}) + \mathbf{M}_{\varepsilon_0\chi^{(3)}\mathbf{e}\mathbf{e}^T}(\mathbf{e}^n - \mathbf{e}^{n-1}) \\ &= \mathbf{M}_{\text{update}}(\mathbf{e}^n - \mathbf{e}^{n-1}),\end{aligned}$$

where $\mathbf{M}_{\text{update}} = \mathbf{M}_{\varepsilon_0(1+\chi^{(1)})} + \mathbf{M}_{\varepsilon_0\chi^{(3)}\|\mathbf{e}\|^2} + \mathbf{M}_{\varepsilon_0\chi^{(3)}\mathbf{e}\mathbf{e}^T}$ and the matrices on the right-hand side are the mass matrices corresponding to weighted $\mathbf{L}^2$ inner products. The matrix $\mathbf{M}_{\text{update}}$ depends on the material parameters ε_0 (permittivity), $\chi^{(1)}$, $\chi^{(3)}$, $\|\mathbf{e}\|^2$ and $\mathbf{e}\mathbf{e}^T$. Since the matrix $\mathbf{M}_{\text{update}}$ depends on the electric field intensity, it has to be updated at each time step, i.e. the mass matrix $\mathbf{M}_{\text{update}}$ is obtained at the time step n by the approximated value of the electric vector $\mathbf{e}^{n-1}$ at the time step $n-1$. $\mathbf{M}_{\text{update}}$ is a positively definite mass matrix with size $\dim\mathbf{U}_{0h} \times \dim\mathbf{U}_{0h}$. Therefore, the general Newton step for the equations (15)–(17) can be written as follows:

$$\frac{\mathbf{d}^n - \mathbf{d}^{n-1}}{\Delta t} = (\mathbf{K})^T \mathbf{h}^n + \mathbf{j}^n, \tag{19}$$

$$\mathbf{d}^n - \mathbf{d}^{n-1} = \mathbf{M}_{\text{update}}(\mathbf{e}^n - \mathbf{e}^{n-1}), \tag{20}$$

$$\mathbf{M}_{\mu_0}\frac{\mathbf{h}^n - \mathbf{h}^{n-1}}{\Delta t} = -\mathbf{K}\mathbf{e}^n. \tag{21}$$

The size of $\mathbf{M}_{\mu_0}$ is $\dim\mathbf{V}_h \times \dim\mathbf{V}_h$, it is also symmetric and positively definite. In general, the vectors $\mathbf{e}^n$ and $\mathbf{h}^n$ have different dimensions $\dim\mathbf{U}_{0h}$ and $\dim\mathbf{V}_h$, respectively. The matrix $\mathbf{K}$ represents a discrete representation of $-\text{curl}$ and has the size $\dim\mathbf{V}_h \times \dim\mathbf{U}_{0h}$. Therefore, $\mathbf{K}$ is a rectangular matrix.

5.1 Implementation of the Energy Conserving Backward Euler-Type Method

The implementation of the energy conserving backward Euler-type method for the nonlinear equations (19)–(21) reads as follows:

Calculate the total number of time steps:

$$nstep := \frac{T - t_0}{\Delta t}$$

Compute the matrices $\mathbf{K}$, $\mathbf{M}_{\mu_0}$ and the initial values of the electric and magnetic fields:

$$\mathbf{e}^0 \leftarrow \mathbf{E}_0$$

$$\mathbf{h}^0 \leftarrow \mathbf{H}_0$$

Loop over the time steps:
`for` $n = 1$ `to` *nstep* `do:`
Begin integration method update:

$$\mathbf{e}_{init} \leftarrow \mathbf{e}^{n-1}$$

$$\mathbf{h}_{init} \leftarrow \mathbf{h}^{n-1}$$

Compute the matrix $\mathbf{M}_{\text{update}}$ and the right-hand side:

$$\begin{pmatrix} \mathbf{f}_{e,init} \\ \mathbf{f}_{h,init} \end{pmatrix} \leftarrow \begin{pmatrix} \mathbf{M}_{\text{update}}\mathbf{e}_{init} + \Delta t \mathbf{j}^n) \\ \mathbf{M}_{\mu_0}\mathbf{h}_{init} \end{pmatrix}$$

Solve the linear system of equations w.r.t. $\mathbf{e}_{out}$, $\mathbf{h}_{out}$:

$$\begin{pmatrix} \mathbf{M}_{\text{update}} & -\Delta t \mathbf{M}_{\mu_0} \\ \Delta t \mathbf{K} & \mathbf{M}_{\mu_0} \end{pmatrix} \begin{pmatrix} \mathbf{e}_{out} \\ \mathbf{h}_{out} \end{pmatrix} = \begin{pmatrix} \mathbf{f}_{e,init} \\ \mathbf{f}_{h,init} \end{pmatrix}$$

Update the electric and magnetic fields values for this time step and compute the energy for given $\chi^{(1)}$ and $\chi^{(3)}$:

$$\mathbf{e}^n \leftarrow \mathbf{e}_{out}$$

$$\mathbf{h}^n \leftarrow \mathbf{h}_{out}$$

$$\mathcal{E}^n \leftarrow \|\mathbf{e}^n\|^2_{\varepsilon_0(1+\chi^{(1)})} + \frac{3}{2}\|(\mathbf{e}^n)^2\|^2_{\varepsilon_0\chi^{(3)}} + \|\mathbf{h}^n\|^2_{\mu_0}$$

`end for`
Completion:

$$\mathbf{e}^N \leftarrow \mathbf{e}^{nstep}$$

$$\mathbf{h}^N \leftarrow \mathbf{h}^{nstep}$$

Example 1: The permittivity, conductivity and the permeability are chosen as $\varepsilon = 1.0$, $\sigma = 0.0$ and $\mu = 2.0$. The susceptibilities $\chi^{(1)}$ and $\chi^{(3)}$ also assume constant values, but may be different in different tests. The electric and magnetic fields are initialized by taking the projections [50, equation (31)] of the exact electric and magnetic fields, where the exact fields given by [59]

$$\mathbf{E} = (-2t-2x, -2t-2y, -2t-2z)^T, \quad \mathbf{B} = (2y-2z, 2z-2x, 2x-2y)^T, \quad \mathbf{J} = (t+x, t+y, t+z)^T.$$

Example 2: This test example is characterized by the following parameters. The permittivity and the permeability are chosen as the constant vacuum values $\varepsilon = \varepsilon_0$ and $\mu = \mu_0$. The susceptibilities $\chi^{(1)}$ and $\chi^{(3)}$ also assume constant values, but may be different in different tests. The angular frequency is $\omega = 2\pi f$ (rad·s^{-1}) with $f = \frac{\sqrt{3}}{2}c_0$ Hz. The exact electric and magnetic fields are given as in [50]:

$$\mathbf{E} = (-\cos(\pi x)\sin(\pi y)\sin(\pi z)\cos(\omega t),\ 0\ ,\ \sin(\pi x)\sin(\pi y)\cos(\pi z)\cos(\omega t))^T,$$

$$\mathbf{B} = \Big(-\frac{\pi}{\omega}\sin(\pi x)\cos(\pi y)\cos(\pi z)\sin(\omega t),\ \frac{2\pi}{\omega}\cos(\pi x)\sin(\pi y)\cos(\pi z)\sin(\omega t),$$
$$-\frac{\pi}{\omega}\cos(\pi x)\cos(\pi y)\sin(\pi z)\sin(\omega t)\Big)^T.$$

If $\chi^{(3)} = 0$ in the system of equations (1)–(4), the problem becomes linear. For this case, error estimates both at semi-discrete and fully discrete levels, energy conservation and simulations have already been demonstrated in [47]–[50]. Here, the efficiency, unconditionally stability with respect to time step, energy stability, robustness of semi-discrete and fully discrete formulation for the nonlinear 3D problem, are presented and discussed by several computational experiments.

A number of numerical experiments are performed to validate the energy conserving properties of the proposed methods, by employing the backward Euler-type and SDIRK23 methods. In

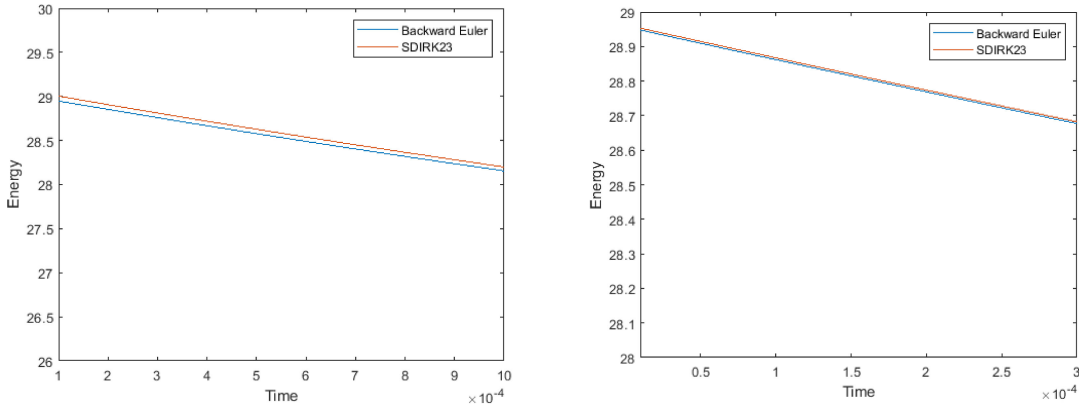

Fig. 1. The energy (18) from $t_0 = 0.0001$ to the final time $T = 0.001$ computed by the backward Euler-type and SDIRK23 methods with time step size $\Delta t = 0.0001$ [Fig. (1a)]. The energy (18) from $t_0 = 0.00001$ to the final time $T = 0.0003$ computed by the backward Euler-type and SDIRK23 methods with time step size $\Delta t = 0.00001$ [Fig. (1b)]. In both figures, the parameters are: $\chi^{(1)} = 3.2222$ and $\chi^{(3)} = 1.5 \times 10^{-19}$.

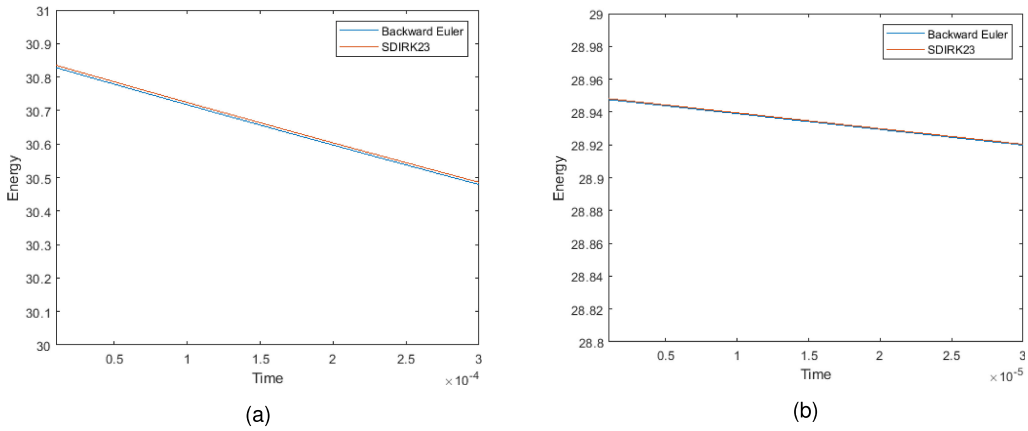

Fig. 2. The energy (18) from $t_0 = 0.00001$ to the final time $T = 0.0003$ computed by the backward Euler-type and SDIRK23 methods with the parameters $\Delta t = 0.00001$, $\chi^{(1)} = 2.2$, and $\chi^{(3)} = 4.1$ [Fig. (2a)]. The energy (18) in Fig. (2b) from $t_0 = 0.000001$ to the final time $T = 0.00003$ computed by the backward Euler-type and SDIRK23 methods with the parameters $\Delta t = 0.000001$, $\chi^{(1)} = 3.2222$, and $\chi^{(3)} = 1.5 \times 10^{-19}$ [Fig. (2b)].

Figs. 1–3, the permittivity, permeability, susceptibilities $\chi^{(1)}$, and $\chi^{(3)}$ also assume constant values to determine the energy (18). The projections [50, equation (31)] of the exact quantities from Example 2 are used to initialize the electric field and magnetic induction, in 1–3. In Fig. 1a, the energy (18) from $t_0 = 0.0001$ to the final time $T = 0.001$ is presented by employing the backward Euler-type and SDIRK23 methods. The time step size is $\Delta t = 0.0001$ in Fig. 1a. Furthermore, in Fig. 1b the energy (18) for the time step size $\Delta t = 0.00001$, from $t_0 = 0.00001$ to the final time $T = 0.0003$, is depicted by employing the backward Euler-type and SDIRK23 methods. The parameters are $\chi^{(1)} = 3.2222$ and $\chi^{(3)} = 1.5 \times 10^{-19}$ in Fig. 1a–b. In Fig. 2a, the susceptibilities $\chi^{(1)} = 2.2$ and $\chi^{(3)} = 4.1$ are chosen, where the time set size is $\Delta t = 0.00001$. The Fig. 2a shows the energy (18) from $t_0 = 0.00001$ to the final time $T = 0.0003$ by using the backward Euler-type and SDIRK23 methods. The energy (18) obtained by the backward Euler-type and SDIRK23 methods from $t_0 = 0.000001$ to the final time $T = 0.00003$ is presented in Fig. 2b; the parameters are $\Delta t = 0.000001$, $\chi^{(1)} = 3.2222$ and $\chi^{(3)} = 1.5 \times 10^{-19}$. The Fig. 3 demonstrates the energy

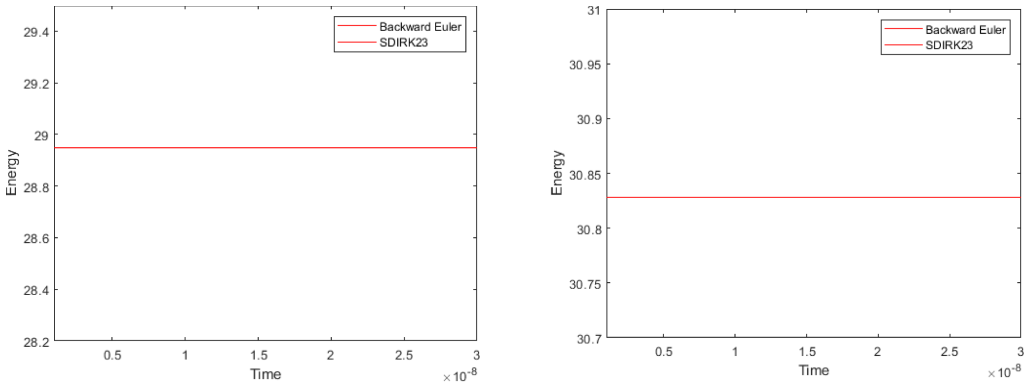

Fig. 3. The energy (18) from $t_0 = 10^{-9}$ to the final time $T = 3 \times 10^{-8}$ computed by the backward Euler-type and SDIRK23 methods. Tthe parameters are: $\chi^{(1)} = 3.2222$, $\chi^{(3)} = 1.5 \times 10^{-19}$ [Fig. (3a)], $\chi^{(1)} = 2.2$, and $\chi^{(3)} = 4.1$ [Fig. (3b)]. In both figures, the time step is $\Delta t = 10^{-9}$.

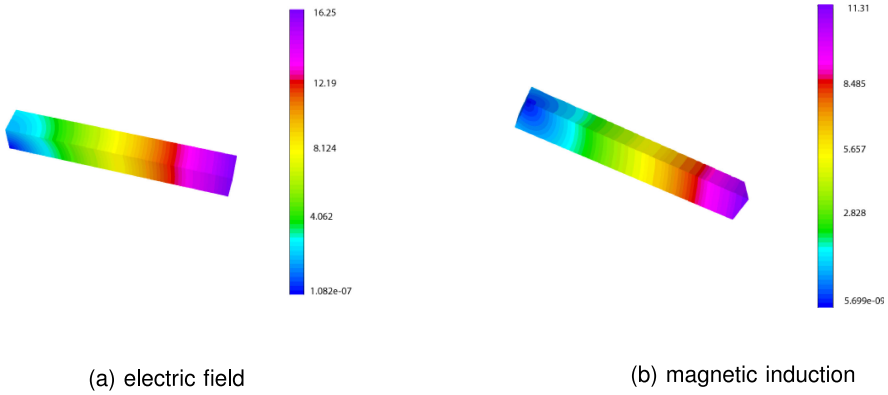

Fig. 4. A snapshot of the electric field (a) and magnetic induction (b) are taken at the final time $T = 10^{-7}$ (number of steps $N = 100$) using the backward Euler-type method for a beam mesh. The parameters are: time step size $\Delta t = 10^{-9}$, $\chi^{(1)} = 2.2$, and $\chi^{(3)} = 4.1$.

(18) from $t_0 = 10^{-9}$ to the final time $T = 3 \times 10^{-8}$ obtained by using the backward Euler-type and SDIRK23 methods with the time step size $\Delta t = 10^{-9}$, where the susceptibility parameters are chosen as $\chi^{(1)} = 3.2222$, $\chi^{(3)} = 1.5 \times 10^{-19}$ (Fig. 3a) and $\chi^{(1)} = 2.2$, $\chi^{(3)} = 4.1$ (Fig. 3b).

Fig. 3 shows that the nonlinear electromagnetic energy computed by backward Euler-type and SDIRK23 methods has the same value for the time step $\Delta t = 10^{-9}$ and different nonlinear parameters. However, it should be noted that the SDIRK23 method, unlike the Euler-type method, is computationally more expensive.

The electric field and magnetic induction are visualized for various 3D meshes (beam, Fichera and Escher). In Figs. 4–7, the electric field and magnetic induction are initialized by taking the projections [50, equation (31)] of the exact quantities from Example 1. The snapshots of the electric field and magnetic induction in Figs. 4–7 present the results obtained using the backward Euler-type method at the time $T = 10^{-7}$, where the time step size is $\Delta t = 10^{-9}$, and the susceptibilities parameters are $\chi^{(1)} = 3.2$ and $\chi^{(3)} = 1.2$. Fig. 4 shows the electric field and magnetic induction values for the beam mesh at the final time. In Fig 5, different orientations of the electric field (Fichera mesh 3D L-shaped domain) at the final time $T = 10^{-7}$ are depicted. Similarly the magnetic induction is presented in Fig. 6 at the final time. Snapshots of the electric field and magnetic induction taken at the final time $T = 10^{-7}$ are presented in Fig. 7 for the Escher meshes.

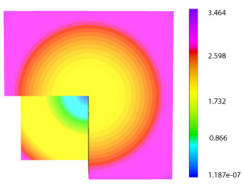

(a) Snapshot from above

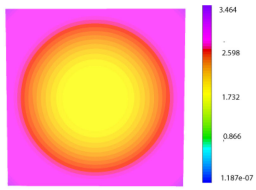

(b) Snapshot from below

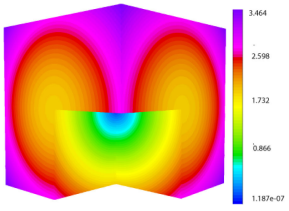

(c) Snapshot from above and front

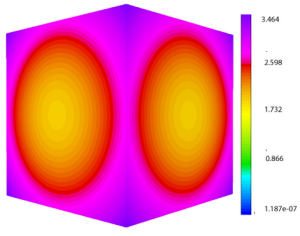

(d) Snapshot from back and below

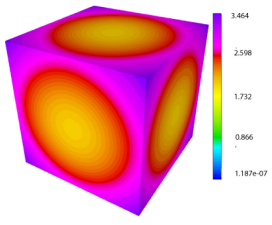

(e) Snapshot from back, left and below

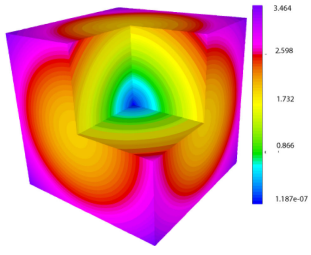

(f) Snapshot from right, front and above

Fig. 5. The snapshots of the electric field are taken at the final time $T = 10^{-7}$ (number of step $N = 100$) using the backward Euler-type method for the Fichera mesh. The parameters are: time step size $\Delta t = 10^{-9}$, $\chi^{(1)} = 2.2$, and $\chi^{(3)} = 4.1$.

In Figs. 8–9, the projections [50, equation (31)] of the exact quantities from Example 2 are used to initialize the electric field and magnetic induction. Figs. 8 and 9 depict the electric field and magnetic induction for a Fichera mesh at the time $T = 0.001$, where the time step size is $\Delta t = 0.00001$, and the susceptibilities parameters are $\chi^{(1)} = 2.2$ and $\chi^{(3)} = 1.5 \times 10^{-19}$.

The Figs. 1–3 illustrate the conservation property of the energy (18) for the nonlinear problem in 3D. We showed that the semi-discretization (12)–(14) along with the backward Euler-type and SDIRK23 methods conserve the energy. The proposed time discretization methods are not restricted to small values of $\Delta t/h$ (Courant-Friedrichs-Lewy condition). Therefore, the proposed methods are unconditionally stable in contrast to many existing methods [13], [26], [43]. Moreover, in the proposed Euler-type time discretization scheme the Newton iterations reduce to a single step at each time step while many existing methods require several Newton iterations at each time step [37]–[39], [42], [43], [45], [46]. Therefore our scheme is computationally more efficient than the a lot of existing methods.

Our proposed methods solve numerically the full system of Maxwell's equations with cubic nonlinearities in 3D directly, whereas many existing methods (SVEA, BPM, the electric field formulation, the magnetic field formulation, $A - \phi$ method, operator form, magnetic vector potential, decoupled schemes and A-Formulation) do not solve the nonlinear problem in Optics and Photonics

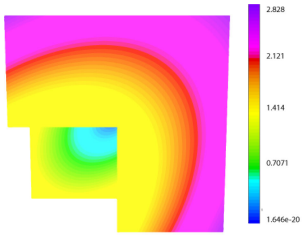

(a) Snapshot from above

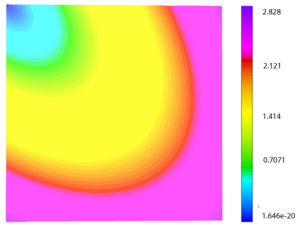

(b) Snapshot from below

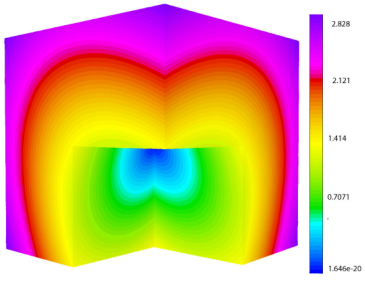

(c) Snapshot from above and front

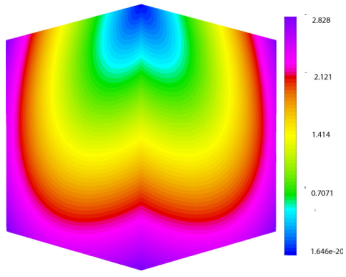

(d) Snapshot from back and below

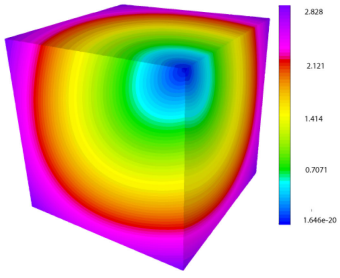

(e) Snapshot from back, left and below

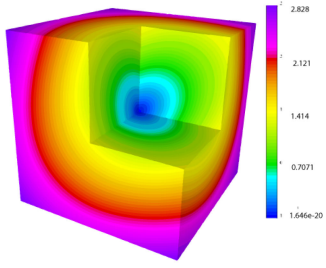

(f) Snapshot from right, front and above

Fig. 6. The snapshots of the magnetic induction are taken at the final time $T = 10^{-7}$ (number of step $N = 100$) using the backward Euler-type method for the Fichera mesh. The parameters are: time step size $\Delta t = 10^{-9}$, $\chi^{(1)} = 2.2$, and $\chi^{(3)} = 4.1$.

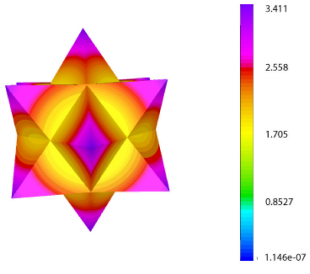

(a) electric field

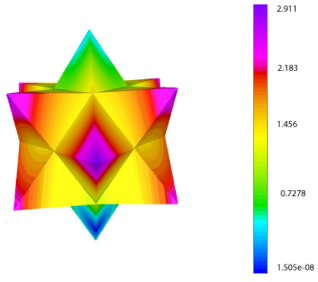

(b) magnetic induction

Fig. 7. A snapshot of the electric field and magnetic induction at the final time $T = 10^{-7}$ (number of steps $N = 100$) using the backward Euler-type method for an Escher mesh is taken. The parameters are: time step size $\Delta t = 10^{-9}$, $\chi^{(1)} = 2.2$, and $\chi^{(3)} = 4.1$.

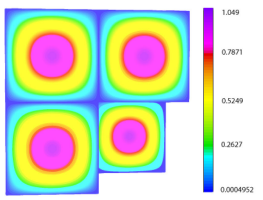

(a) Snapshot from above

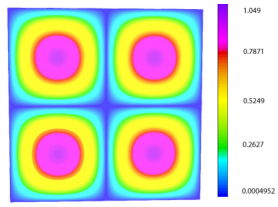

(b) Snapshot from below

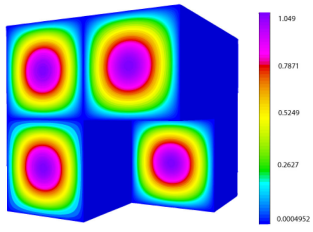

(c) Snapshot from above and front

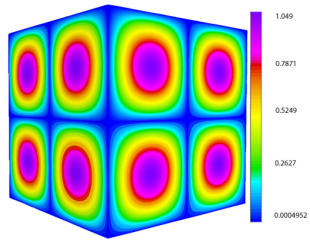

(d) Snapshot from back and below

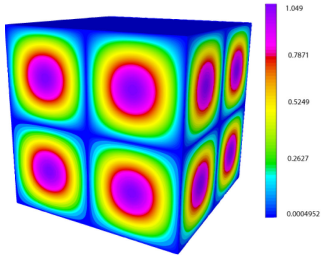

(e) Snapshot from back, left and below

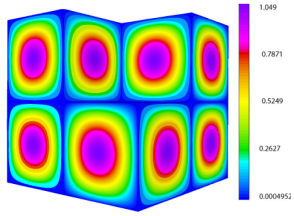

(f) Snapshot from right and front

Fig. 8. The snapshots of the electric field are taken at the final time $T = 0.001$ (number of steps $N = 100$) using the backward Euler-type method for the Fichera mesh. The parameters are: time step size $\Delta t = 0.00001$, $\chi^{(1)} = 2.2$, and $\chi^{(3)} = 1.5 \times 10^{-19}$.

directly [15], [18]–[25], [28], [29], [60] or solve the problem only in 1D and 2D, e.g. [26], [37]–[46]. Those methods do not solve the system of nonlinear Maxwell's equations in Optics and Photonics directly and may cause spurious solutions [26], [50]. In addition, the fully discrete formulations proposed in [43] are only conditionally stable. The TDFEM for nonlinear problems in Electromagnetics proposed in [37]–[39], [42], [45], [46] may also fail to satisfy an energy stability property.

We conclude from the computational experiments presented in this paper that the proposed novel TDFEMs for the full system of nonlinear Maxwell's equation in 3D conserve the energy (at semi-discrete and fully discrete levels), are unconditionally stable (no Courant-Friedrichs-Lewy condition), computationally efficient (one Newton iteration per time step) and figure out the fields (quantities) directly, in contrast to many existing methods (SVEA, BPM, the electric field formulation, the magnetic field formulation, $A - \phi$ method, operator form, magnetic vector potential, decoupled schemes and A-Formulation). In particular, our proposed semi-discrete and fully discrete methods could replace the existing 1D [43] and 2D [45], [46] schemes to 3D, and [39], [42]. Moreover our proposed methods are intermediate results for the theoretical and computational development of energy conserving time-domain discontinuous methods for 3D nonlinear problems in Optics and Photonics. The semi-discrete scheme is also suitable for the application of other higher-order time domain methods e.g. leapfrog, SDIRK34 and symplectic methods.

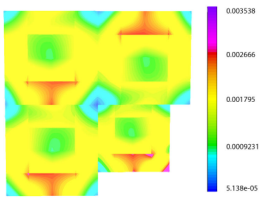

(a) Snapshot from above

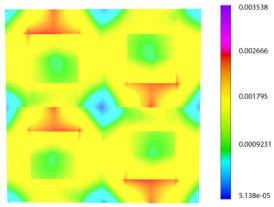

(b) Snapshot from below

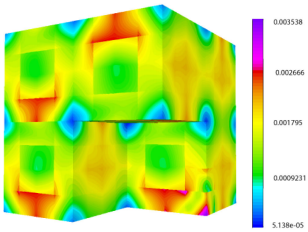

(c) Snapshot from above and front

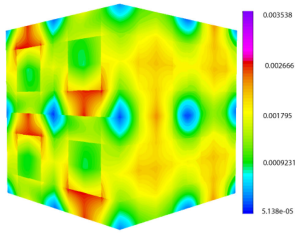

(d) Snapshot from the back and below

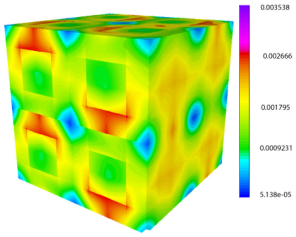

(e) Snapshot from the back, left and below

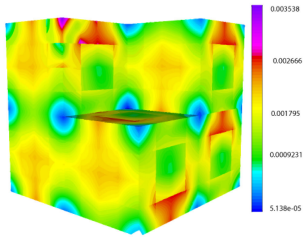

(f) Snapshot from right and front

Fig. 9. The snapshots of the magnetic induction are taken at the final time $T = 0.001$ (number of steps $N = 100$) using the backward Euler-type method for the Fichera mesh. The parameters are: time step size $\Delta t = 0.00001$, $\chi^{(1)} = 2.2$, and $\chi^{(3)} = 1.5 \times 10^{-19}$.

6. Conclusion

For the first time, a new modeling approach has been developed that allows the direct simulation of the full nonlinear Maxwell's equations in Optics and Photonics in 3D. The new capabilities of the proposed method permit that linear and nonlinear effects of the electric polarization in 3D are modeled in an efficient manner that is unconditionally stable and conserves the energy. The novel approach allows energy stability both at the semi-discrete and fully discrete levels, which were not yet available using edge and face elements with the Euler and diagonally implicit Runge-Kutta time discretization for the full system of nonlinear Maxwell's equations in 3D. The approach is almost completely general and could replace SVEA, BPM, the electric field formulation, the magnetic field formulation, $A - \phi$ method, operator form, magnetic vector potential, A-Formulation and decoupled schemes. Numerical results for the energy validate the theoretical findings, which prove that the full discretization is unconditionally stable and conserves the energy.

Acknowledgment

The authors would like to thank Mark L. Stowell and Aaron C. Fisher (Lawrence Livermore National Laboratory, USA) for their valuable suggestions on some implementation issues.

References

[1] R. W. Boyd, *Nonlinear Optics*. New York, NY, USA: Academic, 2003.
[2] N. Bloembergen, *Nonlinear Optics*. Singapore: World Scientific, 1996.
[3] G. New, *Introduction to Nonlinear Optics*. Cambridge, U.K.: Cambridge Univ. Press, 2011.
[4] G. P. Agrawal, *Fiber-Optic Communication Systems*, vol. 222. Hoboken, NJ, USA: Wiley, 2012.
[5] K. Yee, "Numerical solution of initial boundary value problems involving Maxwell's equations in isotropic media," *IEEE Trans. Antennas Propag.*, vol. 14, no. 3, pp. 302–307, May 1966.
[6] R. M. Joseph, S. C. Hagness, and A. Taflove, "Direct time integration of Maxwell's equations in linear dispersive media with absorption for scattering and propagation of femtosecond electromagnetic pulses," *Opt. Lett.*, vol. 16, no. 18, pp. 1412–1414, 1991.
[7] R. W. Ziolkowski and J. B. Judkins, "Full-wave vector Maxwell equation modeling of the self-focusing of ultrashort optical pulses in a nonlinear Kerr medium exhibiting a finite response time," *J. Opt. Soc. America B*, vol. 10, no. 2, pp. 186–198, 1993.
[8] R. M. Joseph and A. Taflove, "FDTD Maxwell's equations models for nonlinear electrodynamics and optics," *IEEE Trans. Antennas Propag.*, vol. 45, no. 3, pp. 364–374, Mar. 1997.
[9] A. Taflove and S. C. Hagness, *Computational Electrodynamics: The Finite-Difference Time-Domain Method*. Boston, MA, USA: Artech House, 2005.
[10] M. Fujii, M. Tahara, I. Sakagami, W. Freude, and P. Russer, "High-order FDTD and auxiliary differential equation formulation of optical pulse propagation in 2-D Kerr and Raman nonlinear dispersive media," *IEEE J. Quantum Electron.*, vol. 40, no. 2, pp. 175–182, Feb. 2004.
[11] J. H. Greene and A. Taflove, "General vector auxiliary differential equation finite-difference time-domain method for nonlinear optics," *Opt. Express*, vol. 14, no. 18, pp. 8305–8310, 2006.
[12] G. Cohen and S. Pernet, *Finite Element and Discontinuous Galerkin Methods for Transient Wave Equations*. Berlin, Germany: Springer, 2017.
[13] M. Moradi, S.-M. Pourangha, V. Nayyeri, M. Soleimani, and O. M. Ramahi, "Unconditionally stable FDTD algorithm for 3-D electromagnetic simulation of nonlinear media," *Opt. Express*, vol. 27, no. 10, pp. 15 018–15 031, 2019.
[14] P. M. Goorjian, A. Taflove, R. M. Joseph, and S. C. Hagness, "Computational modeling of femtosecond optical solitons from Maxwell's equations," *IEEE J. Quantum Electron.*, vol. 28, no. 10, pp. 2416–2422, Oct. 1992.
[15] R. M. Joseph, P. M. Goorjian, and A. Taflove, "Direct time integration of Maxwell's equations in two-dimensional dielectric waveguides for propagation and scattering of femtosecond electromagnetic solitons," *Opt. Lett.*, vol. 18, no. 7, pp. 491–493, 1993.
[16] R. W. Ziolkowski and J. B. Judkins, "Applications of the nonlinear finite difference time domain (NL-FDTD) method to pulse propagation in nonlinear media: Self-focusing and linear-nonlinear interfaces," *Radio Sci.*, vol. 28, no. 5, pp. 901–911, 1993.
[17] R. W. Ziolkowski and J. B. Judkins, "Nonlinear finite-difference time-domain modeling of linear and nonlinear corrugated waveguides," *J. Opt. Soc. America B*, vol. 11, no. 9, pp. 1565–1575, 1994.
[18] P. M. Goorjian and A. Taflove, "Direct time integration of Maxwell's equations in nonlinear dispersive media for propagation and scattering of femtosecond electromagnetic solitons," *Opt. Lett.*, vol. 17, no. 3, pp. 180–182, 1992.
[19] C. V. Hile and W. L. Kath, "Numerical solutions of Maxwell's equations for nonlinear-optical pulse propagation," *J. Opt. Soc. America B*, vol. 13, no. 6, pp. 1135–1145, 1996.
[20] A. Bourgeade and B. Nkonga, "Numerical modeling of laser pulse behavior in nonlinear crystal and application to the second harmonic generation," *Multiscale Model. Simul.*, vol. 4, no. 4, pp. 1059–1090, 2005.
[21] M. P. Sørensen, G. M. Webb, M. Brio, and J. V. Moloney, "Kink shape solutions of the Maxwell-Lorentz system," *Phys. Rev. E*, vol. 71, no. 3, 2005, Art. no. 036602.
[22] M. Pototschnig, J. Niegemann, L. Tkeshelashvili, and K. Busch, "Time-domain simulations of the nonlinear Maxwell equations using operator-exponential methods," *IEEE Trans. Antennas Propag.*, vol. 57, no. 2, pp. 475–483, Feb. 2009.
[23] S. Nagaraj, J. Grosek, S. Petrides, L. F. Demkowicz, and J. Mora, "A 3D DPG Maxwell approach to nonlinear Raman gain in fiber laser amplifiers," *J. Comput. Phys.: X*, vol. 2, 2019, Art. no. 100002.
[24] P. Kinsler, S. Radnor, J. Tyrrell, and G. New, "Optical carrier wave shocking: Detection and dispersion," *Phys. Rev. E*, vol. 75, no. 6, 2007, Art. no. 066603.
[25] J. Tyrrell, P. Kinsler, and G. New, "Pseudospectral spatial-domain: A new method for nonlinear pulse propagation in the few-cycle regime with arbitrary dispersion," *J. Modern Opt.*, vol. 52, no. 7, pp. 973–986, 2005.
[26] A. Fisher, D. White, and G. Rodrigue, "An efficient vector finite element method for nonlinear electromagnetic modeling," *J. Comput. Phys.*, vol. 225, no. 2, pp. 1331–1346, 2007.
[27] T. Fujisawa and M. Koshiba, "Time-domain beam propagation method for nonlinear optical propagation analysis and its application to photonic crystal circuits," *J. Lightw. Technol.*, vol. 22, no. 2, pp. 684–691, Feb. 2004.
[28] A. de La Bourdonnaye, "High-order scheme for a nonlinear Maxwell system modelling Kerr effect," *J. Comput. Phys.*, vol. 160, no. 2, pp. 500–521, 2000.
[29] D. Aregba-Driollet, "Godunov scheme for Maxwell's equations with Kerr nonlinearity," *Commun. Math. Sci.*, pp. 2195–2222, 2015.
[30] J. S. Hesthaven and T. Warburton, "Nodal high-order methods on unstructured grids: I. Time-domain solution of Maxwell's equations," *J. Comput. Phys.*, vol. 181, no. 1, pp. 186–221, 2002.
[31] B. Cockburn, F. Li, and C.-W. Shu, "Locally divergence-free discontinuous Galerkin methods for the Maxwell equations," *J. Comput. Phys.*, vol. 194, no. 2, pp. 588–610, 2004.
[32] E. T. Chung and B. Engquist, "Optimal discontinuous Galerkin methods for wave propagation," *SIAM J. Numer. Anal.*, vol. 44, no. 5, pp. 2131–2158, 2006.

[33] E. T. Chung, P. Ciarlet Jr, and T. F. Yu, "Convergence and superconvergence of staggered discontinuous Galerkin methods for the three-dimensional Maxwell's equations on Cartesian grids," *J. Comput. Phys.*, vol. 235, pp. 14–31, 2013.
[34] R. Abedi and S. Mudaliar, "An asynchronous spacetime discontinuous Galerkin finite element method for time domain electromagnetics," *J. Comput. Phys.*, vol. 351, pp. 121–144, 2017.
[35] Y. Huang, J. Li, and W. Yang, "Interior penalty DG methods for Maxwell's equations in dispersive media," *J. Comput. Phys.*, vol. 230, no. 12, pp. 4559–4570, 2011.
[36] S. Lanteri and C. Scheid, "Convergence of a discontinuous Galerkin scheme for the mixed time-domain Maxwell's equations in dispersive media," *IMA J. Numer. Anal.*, vol. 33, no. 2, pp. 432–459, 2013.
[37] S. Yan and J.-M. Jin, "Time-domain nonlinear finite element analysis of air breakdown using a simplified plasma model," in *Proc. IEEE Int. Symp. Antennas Propag. USNC/URSI Nat. Radio Sci. Meeting*, 2015, pp. 1824–1825.
[38] S. Yan and J.-M. Jin, "Time-domain finite element modeling of nonlinear conductivity using Newton's method," in *Proc. IEEE Int. Symp. Antennas Propag. USNC/URSI Nat. Radio Sci. Meeting*, 2015, pp. 1822–1823.
[39] S. Yan and J.-M. Jin, "Theoretical formulation of a time-domain finite element method for nonlinear magnetic problems in three dimensions," *Progress Electromagn. Res.*, vol. 153, pp. 33–55, 2015.
[40] B. Zhu, H. Yang, and J. Chen, "A novel finite element time domain method for nonlinear Maxwell's equations based on the parametric quadratic programming method," *Microw. Opt. Technol. Lett.*, vol. 57, no. 7, pp. 1640–1645, 2015.
[41] N. Liu, G. Cai, C. Zhu, Y. Huang, and Q. H. Liu, "The mixed finite-element method with mass lumping for computing optical waveguide modes," *IEEE J. Sel. Topics Quantum Electron.*, vol. 22, no. 2, pp. 187–195, Mar./Apr. 2015.
[42] S. Yan and J.-M. Jin, "A fully coupled nonlinear scheme for time-domain modeling of high-power Microwave air breakdown," *IEEE Trans. Microw. Theory Techn.*, vol. 64, no. 9, pp. 2718–2729, Sep. 2016.
[43] V. A. Bokil, Y. Cheng, Y. Jiang, and F. Li, "Energy stable discontinuous Galerkin methods for Maxwell's equations in nonlinear optical media," *J. Comput. Phys.*, vol. 350, pp. 420–452, 2017.
[44] J. Huang and C.-W. Shu, "A second-order asymptotic-preserving and positivity-preserving discontinuous Galerkin scheme for the Kerr–Debye model," *Math. Models Methods Appl. Sci.*, vol. 27, no. 3, pp. 549–579, 2017.
[45] D. S. Abraham and D. D. Giannacopoulos, "A convolution-free mixed finite-element time-domain method for general nonlinear dispersive media," *IEEE Trans. Antennas Propag.*, vol. 67, no. 1, pp. 324–334, Jan. 2019.
[46] D. S. Abraham and D. D. Giannacopoulos, "A perfectly matched layer for the nonlinear dispersive finite-element time-domain method," *IEEE Trans. Magn.*, vol. 55, no. 6, Jun. 2019, Art. no. 7400804.
[47] A. Anees and L. Angermann, "A mixed finite element method approximation for the Maxwell's equations in Electromagnetics," in *Proc. IEEE Int. Conf. Wireless Inf. Technol. Syst. Appl. Comput. Electromagn. Soc.*, 2016, pp. 179–180.
[48] A. Anees and L. Angermann, "Mixed finite element methods for the Maxwell's equations with matrix parameters," in *Proc. Int. Appl. Comput. Electromagn. Soc. Symp.*, Mar. 24–29, 2018, pp. 1–2.
[49] A. Anees and L. Angermann, "Time-domain finite element methods for Maxwell's equations in three dimensions," in *Proc. Int. Appl. Comput. Electromagn. Soc. Symp.*, Mar. 24–29, 2018, pp. 1–2.
[50] A. Anees and L. Angermann, "Time domain finite element method for Maxwell's equations," *IEEE Access*, vol. 7, pp. 63 852–63 867, 2019.
[51] J.-C. Nédélec, "Mixed finite elements in $\mathbb{R}^3$," *Numerische Mathematik*, vol. 35, no. 3, pp. 315–341, 1980.
[52] J.-C. Nédélec, "A new family of mixed finite elements in $\mathbb{R}^3$," *Numerische Mathematik*, vol. 50, no. 1, pp. 57–81, 1986.
[53] P.-A. Raviart and J.-M. Thomas, "A mixed finite element method for 2-nd order elliptic problems," in *Mathematical Aspects of Finite Element Methods*, Berlin, Germany: Springer, 1977, pp. 292–315.
[54] V. Girault and P. Raviart, *Finite Element Methods for Navier-Stokes Equations*. Berlin, Germany: Springer-Verlag, 1986.
[55] P. G. Ciarlet, *The Finite Element Method for Elliptic Problems*. Philadelphia, PA, USA: SIAM, 2002.
[56] P. Monk, *Finite Element Methods for Maxwell's Equations*. London, U.K.: Oxford Univ. Press, 2003.
[57] E. Hairer and G. Wanner, *Solving Ordinary Differential Equations II. Stiff and Differential-Algebraic Problems*. Berlin, Germany: Springer, 1996.
[58] "MFEM: Modular finite element methods library," [Online]. Available: https://mfem.org
[59] C. Ma, "Convergence of finite element A-ϕ method for solving time-dependent Maxwell's equations," *Appl. Math. Computation*, vol. 176, no. 2, pp. 621–631, 2006.
[60] R. Jestädt, M. Ruggenthaler, M. J. Oliveira, A. Rubio, and H. Appel, "Light-matter interactions within the Ehrenfest–Maxwell–Pauli–Kohn–Sham framework: Fundamentals, implementation, and nano-optical applications," *Advances Phys.*, vol. 68, no. 4, pp. 225–333, 2019.